ACS APPLIED MATERIALS & INTERFACES

Research Article

www.acsami.org

Conducting Instant Adhesives by Grafting of Silane Polymer onto Expanded Graphite

Titash Mondal,[†] Anil K. Bhowmick,*[,†,‡] and Ramanan Krishnamoorti*[,§]

[†]Department of Chemistry, Indian Institute of Technology Patna, Patna, Bihar 800013, India

[‡]Rubber Technology Center, Indian Institute of Technology, Kharagpur 721302, India

[§]Department of Chemical and Biomolecular Engineering, University of Houston, Houston, Texas 77204, United States

Supporting Information

ABSTRACT: A "grafting to" methodology for the attachment of a silane based polymer (SG) onto functionalized graphitic platelets is demonstrated. The siloxy end groups of the modifier were further cross-linked without addition of any external curative. These sterically stabilized nanoplatelets with a high grafting density ensured complete screening of the attractive interparticle interactions. As a result, a better dispersion of platelets was observed compared to the physically mixed platelets in the polymer matrix (SUG). The larger size of the polymer tethered graphitic particles and the greater extent of heat liberated due to grafting resulted in a higher enthalpic contribution in the case of SG compared to SUG. This makes the formation of SG thermodynamically more favorable compared to SUG. Presence of a hierarchical spatial arrangement with a good dispersion of graphitic platelets was observed within the siloxane matrix in the case of SG compared to SUG. The nanoparticle tethered composite generated exhibited an "instant" conducting adhesive behavior. The adhesive properties of the SG were found to be increased due to grafting of graphitic platelets when compared with the neat polymer. Further, SG exhibited a conductive character whereas the neat polymer and SUG demonstrated an insulating character.

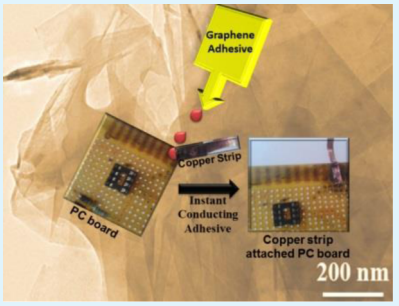

KEYWORDS: *graphene, silane modification, conducting adhesive, nanocomposite*

INTRODUCTION

Properties like the excellent mechanical, optical, thermal and electrical properties[1−3] of graphitic materials make them an object of wide interest. Graphitic materials have uses in a variety of applications ranging from solar cells to polymer nanocomposites[4−7] due to their large surface area with a hexagonal lattice array of sp^2 hybridized carbon atoms. However, the poor dispersibility and solubility of pristine graphitic materials in organic solvents often limits their use in applications. Thus, significant advances in the surface modification of graphitic materials by covalent and noncovalent routes are adopted.[8,9] Polymers are one of the most commonly used materials for surface modification of graphitic materials using noncovalent and covalent methodologies.[10−12] The covalent route is preferentially selected over the noncovalent method, as in the latter case, the graphitic materials are poorly wetted by polymeric chains. As a result, a poorly dispersed system is observed.[13]

The covalent modification of graphitic materials by polymers and functional molecules can be broadly achieved by "grafting from" and "grafting to" techniques. In the case of the "grafting from" technique, the initiator used for polymerization is normally immobilized onto the basal plane and edges of graphitic materials. However, in the case of the "grafting to" technique, covalent linkages between the polymeric/monomeric unit and graphitic oxide (GO) are achieved via amidation or esterification reactions.[11,14] The electrical application of such polymer nanocomposites is often limited due to the insulating nature of GO.[15]

Polymer nanocomposites, due to their superior properties (viz. mechanical, electrical, etc.) compared to the neat polymer, have applications in multiple dimensions.[16] One such popular application relates to the development of electrically conducting adhesives (ECAs).[17] The widespread recognition of ECAs over traditional adhesives (eutectic mixture of lead and tin) is due to the less hazardous environmental impact associated with it. Conducting materials like metal, carbon black, carbon nanotubes, carbon nanofibers and graphite (or a hybrid of them) are used as the nanophase in the matrix.[18−20] A 50−70% filler volume is required when only metal particles are used for this purpose.[21] This causes an increase in the price of metal nanoparticle based ECAs. Thus, efforts have been made in minimizing the usage of metal particles by substituting them with carbon nanomaterials. Both carbon nanotube and graphite based epoxy adhesives have been reported to be prepared using a three roll milling technique, solvent casting technique and emulsification methodology.[22−24] Despite a wide span of research achieved in synthesizing conducting adhesive by the

Received: June 23, 2014
Accepted: September 3, 2014
Published: September 3, 2014

Scheme 1. Proposed Scheme for the Formation of SG from XG Assisted via Coupling Agent DCC

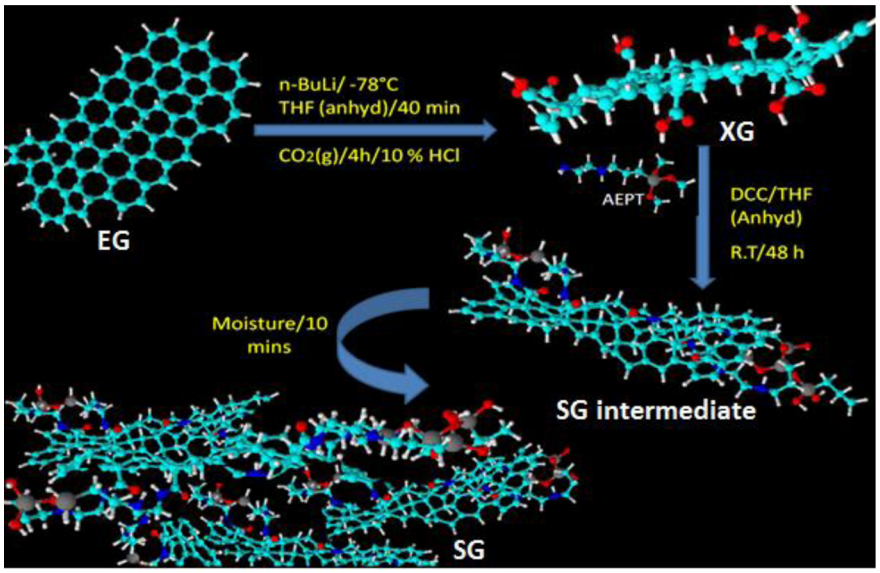

aforementioned techniques, few[25,26] have demonstrated such materials using the "grafting to" technique with special emphasis on graphitic materials. Further, a major section of the work reported in literature deals with epoxy material as the adhesive phase. However, based on our knowledge, reports on graphite-silicone based conducting adhesive matrix are not reported. Apart from that, the entire polymeric composite accounted above requires external curing agent. These curing agents are reported to induce defect and reduce the conductivity of the graphitic platelets.[27] These issues led us to address some of these common unexplored areas.

Here we demonstrate the successful synthesis of graphite-silicone polymer nanocomposite using "grafting to" methodology. The carboxylated graphitic material (XG) with low defect density was selected as the precursor material for this present study.[28] [3-(2-Aminoethylamino)propyl]-trimethoxysilane (AEPT), which is well-known for its adhesive property,[29] was grafted onto XG using amidation reaction. The experimental protocol was designed to ensure that the pendant siloxyl functional groups can be cross-linked in the presence of moisture (noninert conditions). This necessarily avoided the usage of any additional curative. Further, the modified system (SG) was compared and contrasted against a system generated by physical mixing of unmodified graphitic platelets and silane polymer (SUG). The factors affecting the dispersion of the nanophase in the case of SG and SUG have been demonstrated in terms of thermodynamics. Further, dispersion related properties like conductivity and mechanical properties of SG and SUG were also estimated using a standard protocol. The effect of grafting of graphitic platelets on the adhesive behavior of the polymer was also demonstrated by performing the 180° single lap shear test and the performance of the grafted material was compared with the neat polymer. Thus, by combining the electrical conductivity of graphene platelets and the adhesive property of the modifier, a conducting adhesive can be expected. This made the current material superior to the epoxy based adhesives, wherein epoxies are well-known for their affinity toward moisture.[30] This clearly distinguishes the current system from the traditional materials reported in literature.

EXPERIMENTAL SECTION

Materials. Expanded graphite-3777 (EG) was procured from Asbury Carbon, USA. [3-(2-Aminoethylamino)propyl]-trimethoxysilane (AEPT), anhydrous tetrahydrofuran (THF), *N,N′*-dicyclohexylcarbodiimide (DCC) were procured from Sigma-Aldrich, USA. 2.0 M *n*-Butyl lithium (*n*-BuLi) was procured from Sigma-Aldrich, USA. All the above-mentioned chemicals were used without further purification.

Method. *Synthesis and Characterization of Carboxylated Graphene Platelets (XG).* XG was synthesized by using a methodology mentioned elsewhere.[28] Briefly, the synthesis includes the following steps. A 100 mg sample of EG was dispersed in anhydrous tetrahydrofuran (THF; 10 mL). It was sonicated under an inert atmosphere (N_2 gas). Further, the reaction mixture was maintained at −78 °C using an OPERON low temperature reactor. To it, an excess of *n*-BuLi (5 mL) was added dropwise under a nitrogen atmosphere. The mixture was allowed to stir for 40 min. Further to it, carbon dioxide gas was then introduced slowly over a period of 4 h at room temperature. The product was isolated and filtered using 0.22 μm polytetrafluoroethylene membrane filter paper. To this isolated product, 10% hydrochloric acid was added and the mixture was allowed to stir for 2 h. The product was filtered and dried in a vacuum oven for 48 h. The success of the functionalization reaction was analyzed using various spectroscopic techniques like Fourier transform infrared (FTIR; PerkinElmer 400 machine, USA) and Raman spectroscopy (Technos Instrument, India). The change in the local density of state was calculated using scanning tunnelling microscopy (NanoRev, Quazar Technology, India). All the relevant discussions related to synthesis and characterization of XG are incorporated in the Supporting Information section.

Synthesis and Characterization of Silane Modified XG (SG). To graft the silane moiety onto XG, an amidation reaction was utilized. Briefly, 50 mg of XG was taken in 10 mL of anhydrous THF under inert atmosphere. To it, molar excess of AEPT was introduced along with a catalytic amount of DCC, as shown in Scheme 1. The reaction mixture was allowed to stir at 40 °C for 48 h. The obtained product (SG) was in the liquid phase. It was centrifuged at 2000 rpm for 2 min, so as to separate out the unreacted XG. The supernatant solution was collected, and solvent evaporation was done using a rotary evaporator. Interestingly, the mixture solidified within a short span of time after its exposure to a noninert condition. The isolated product was characterized by various techniques. FTIR spectroscopy was used to understand the chemical changes taking place due to functionalization with a resolution of 2 cm^{-1} using the ATR mode. X-ray photoelectron spectroscopy (XPS) measurements of the samples were taken using a

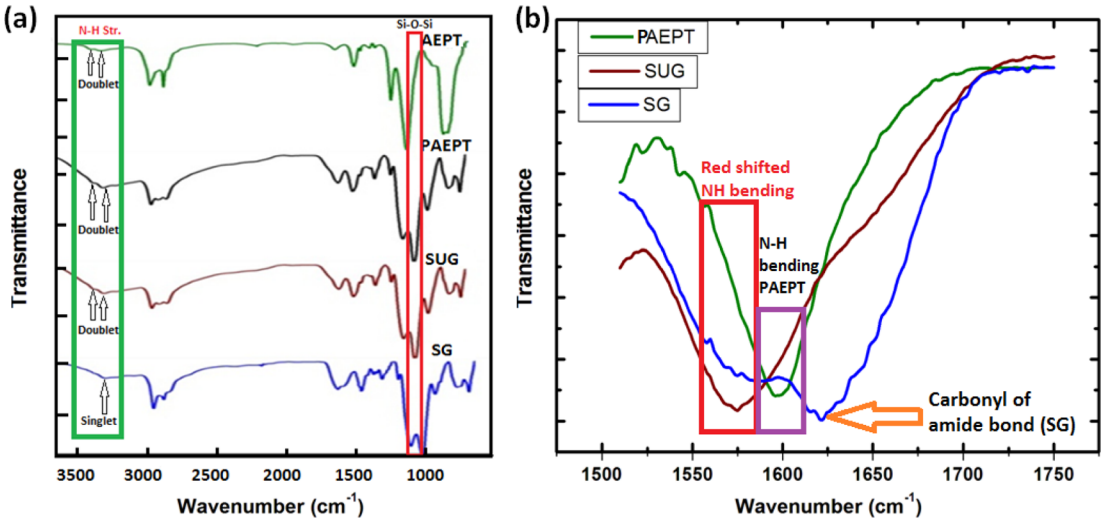

Figure 1. (a) FTIR spectra of AEPT, PAEPT SUG and SG recorded using ATR technique with diamond as the crystal. The spectra were recorded with a resolution of 2 cm^{-1} and 64 scans. A spectrum of air was taken as the background for the analysis. (b) Selective area spectra of PAEPT, SUG and SG recorded under similar conditions.

VG scientific ESCA Lab II spectrometer with an electrostatic lens mode (pass energy of 160 eV; Mg Kα radiation as an excitation source). The X-ray diffraction (XRD) data for the SG were obtained using a Rigaku TT RAX 3 XRD machine with a Cu target (Cu Kα radiation source; λ = 0.154 nm) in the range of 2θ from 10 to 60°. The thermal behavior of the composite was assessed using thermogravimetric analysis (TGA) done in an inert atmosphere (N_2 gas) from room temperature to 800 °C with a ramp rate of 10 °C/min (SD Q600 TA Instruments). Scanning electron microscopy (SEM) was done for SG (FESEM S4800 Hitachi). Atomic force microscopy (AFM) was done in contact mode on spin coated sample using Agilent AFM 5500. The nature of exfoliation of graphitic particles inside the polymeric matrix was studied using high resolution transmission electron microscopy (HRTEM, Technai, FEI instruments) at 300 kV. The electrical response of the composite was determined from the current–voltage (I–V) plots measured using standard four probe measurement technique (Keithley instruments).

Preparation and Characterization of Physical Mixture of AEPT and XG (SUG). Briefly, EG (50 mg) was taken in anhydrous THF (10 mL) and a molar excess of AEPT was introduced to the system in the presence of DCC under the inert atmosphere. Conditions maintained during preparation of the current nanocomposite were kept identical to those for SG. The obtained product, SUG, also solidified like SG upon exposure to a noninert condition at room temperature. To note the changes taking place in polymer nanocomposite with respect to neat polymer, an equal weight of monomer AEPT was taken and was polymerized in a noninert condition. The polymer thus formed was also further characterized.

Mechanical Properties of the Polymer Nanocomposites and Lap Shear Test for Adhesion. The mechanical properties of SG and SUG were estimated using a universal testing machine (Zwick Reoll, Germany) under tension mode. A load cell of 50 N was used for tensile test with a speed of 20 mm/min at room temperature. The tensile strength and elongation at break were estimated from the stress–strain plot. Similarly, the adhesive property of the sample was determined by measuring the force required to tear apart the samples adhered using single lap shear mode. Test strips made out of canvas cloth were prepared. The bonded area was subjected to a load of 2 kg for a developing time of 10 h. The lap shear test was performed by inserting 25 mm of unbonded region of the sample strip on each of the grip. Further, the analysis was performed with a load cell of 50 N and a speed of 25 mm/min.

RESULTS AND DISCUSSION

Synthesis and Characterization of Silane Modified XG (SG). In the present case, carboxylation of expanded graphite was achieved using techniques described elsewhere.[28] These carboxylated graphitic platelets were then subjected to treatment with the AEPT monomer in the presence of DCC. The choice of DCC as the coupling agent was made so as to avoid unwanted acid–base side reactions between amine terminal of AEPT and the proton from carboxylic functionality from XG as shown in Scheme 1. The mechanistic pathway is given in Scheme S1 in the Supporting Information section. As shown in step 1 of Scheme S1, the lone pair of electrons on the nitrogen of DCC participated in the deprotonation of carboxylic functionality of XG. The carboxylate anion generated as the intermediate in step 2 acted as a nucleophile and attacked the carbon center of DCC. This alleviated the positive charge developed on the nitrogen center of DCC. The adduct (A-1) generated in the reaction medium converted the carboxylate anion to a good leaving group. As a result, when AEPT was incorporated into the reaction mixture, the primary amine of AEPT participated in nucleophilic attack on the carbonyl center of A-1. Further, via a tetrahedral intermediate and proton transfer reaction, the monomer-g-XG was formed. When, the monomer-g-XG was introduced to a noninert condition, it underwent a poly condensation reaction to form SG, as shown in Scheme S1.

FTIR spectroscopy in ATR mode was done for all the starting materials as well as for the products formed. EG was not associated with any noticeable spectral pattern. However, the FTIR spectra of XG was marked by the presence of peaks at 1690 cm^{-1} (C═O str. of carboxylic acid), 2920 cm^{-1} (CH_2 str.) and 3690 cm^{-1} (OH str. of carboxylic group), as shown in the Supporting Information, Figure S1. Further, the FTIR spectra for SG, SUG, monomer AEPT and polymeric AEPT (PAEPT) were recorded under similar conditions. The spectrum for AEPT was marked by the presence of doublet peaks in the vicinity of 3360 cm^{-1} (symmetric N—H stretch of 1° amine) and 3440 cm^{-1} (asymmetric N—H stretch of 1° amine), as shown in Figure 1a. Other notable peaks are observed at around 2900 cm^{-1} (–CH_2 stretching), 1597 cm^{-1}

dx.doi.org/10.1021/am5040472 | ACS Appl. Mater. Interfaces 2014, 6, 16097–16105

(N—H bending) and 1450 cm^{-1} (attributed to the scissoring of CH_2 group). The peak at 1076 cm^{-1} is due to Si—O—CH_3 linkages. Doublet peaks for the monomer reduced to a singlet peak at 3312 cm^{-1} for SG, as shown in Figure 1a. Complete utilization of the primary amine for generation of amide bond was indicated from the above observation. However, presence of the peak in that range is due to the secondary amine. The peak at 1625 cm^{-1} is attributed to the amide bond formation taking place between the primary amine of AEPT and the COOH group of XG (marked by orange arrow) as shown in Figure 1b. The peak for N—H bending mode was observed in the vicinity of 1575 cm^{-1}. Presence of peak at 1021 cm^{-1} is due to the formation of Si—O—Si bond (support for formation a of polymer matrix) aided by moisture present in the atmosphere.

Essentially, the peak observed for SG at 1625 cm^{-1} was missing for SUG. This indicated the absence of an amide bond. However, the peak due to the N−H bending mode was still observed in the case of SUG. Presence of doublet peaks near 3300 and 3400 cm^{-1} in the case of PAEPT suggests a free primary amine group. Interestingly, the peak for N−H bending (secondary amine) for SG and SUG was observed to be red-shifted compared to that of the pure polymer (as shown in red box in Figure 1b). This is attributed to the intermolecular hydrogen bonding taking place between the defect side hydrogen of graphitic structure and NH of the polymeric phase. The other notable difference is the peak position for the Si−O−Si bond (as shown in the red box in Figure 1a). In the case of SUG, the peak for the Si−O−Si bond was observed at 1037 cm^{-1}. The shift in the Si−O−Si peak position by 9 cm^{-1} is significant, thereby suggesting a positive interaction between the filler and the polymer matrix. On the contrary, the spectrum for SUG was almost identical to that of PAEPT, suggesting a lack of any notable interactions between the filler and the polymer with respect to the Si−O−Si linkages as shown in Figure 1. The data set reported for FTIR spectroscopy is based on the average of three different experiments performed.

The shift in the peak for Si−O−Si is explainable in terms of the enthalpic contribution. The formation of siloxane is mediated via a condensation reaction of the AEPT to form stable Si−O−Si linkages. As a result, methanol will be removed from the reaction medium as the byproduct. This causes release of heat (negative value of enthalpy of condensation, ΔH_{cond}) from the medium due to the formation of PAEPT. A similar phenomenon is expected to take place for SG and SUG. However, in the case of SG, grafting of XG onto polymeric chains results in release of dicyclohexyl urea and methanol from the reaction medium. As a result, the value for enthalpy of condensation is expected to be more negative due to the release of greater extent of low molecular weight fragments. However, in the case of SUG, the loss of a low molecular weight fraction is similar to that of formation of PAEPT. Thus, it can be surmised that the formation of SG will be associated with greater extent of heat compared to the formation of PAEPT and SUG. Further, nanoparticles have an insertion enthalpy (H) that scales up with the increase in the surface area ($A = 4\pi a^2$) where a is the radius of the nanoparticles, expressed as[31]

$$H \sim 4\pi a^2 \tag{1}$$

Thus, from the above equation, it is expected that grafting of polymeric moiety onto XG in the case of SG will tend to increase the surface area of a nanomaterial. However, in the case of SUG, the contribution made by nanoparticle will be governed only by the surface area of the unfunctionalized graphite. As a result, the enthalpic contribution is more in the case of SG compared to SUG. Further, the higher extent of enthalpic contribution for SG can be expressed in terms of particle−particle and particle−polymer interaction. In case of SG, only a fractional area (A_c) of functionalized platelets will be in molecular contact due to van der Waals force (σ) acting on it as expressed below

$$A_c = \left(\frac{Z\sigma}{4a}\right) \times A \tag{2}$$

where Z is the average coordination number of the nanoparticle aggregate. The uncovered platelet surface area (A_U, vide infra) does not have favorable interactions with each other

$$A_U \equiv A - A_c \tag{3}$$

However, the contact of graphitic platelets with the polymer gets enthalpically favorable and a better dispersion is resulted in the case of SG. Such a kind of favorable interaction has been reported by using the PRISM site model by Hooper and Schweizer.[32] On the other hand, in the case of SUG, due to a lack of notable intercalation of the monomer moiety in between the graphitic platelets, the surface of a nanomaterial is not exposed to the polymer. As a result, such a type of enthalpic stabilization is not possible. Further, the shift in the FTIR peak position of the Si−O−Si linkage can be correlated with the enthalpic contribution ($\Delta H_{composite}$) value using Fowke's equation[33]

$$\Delta H_{composite} = 0.236 \times \Delta \upsilon_{Si-O-Si} \tag{4}$$

where $\Delta\upsilon$ is the shift in the frequency of the Si−O−Si stretching vibration corresponding to the pure polymer. The $\Delta H_{composite}$ value for SG was found to be −2.1 kcal/mol, whereas the $\Delta H_{composite}$ value for SUG was obtained as −0.2 kcal/mol considering the peak for Si−O−Si linkage. Thus, it can be concluded that formation of SG was thermodynamically more favorable compared to SUG.

Further, the thermal analysis of AEPT, SUG and PAEPT was carried out from room temperature to 680 °C using a nitrogen atmosphere, as shown in Figure 2. The monomer was significantly degraded in the vicinity of 200 °C. However,

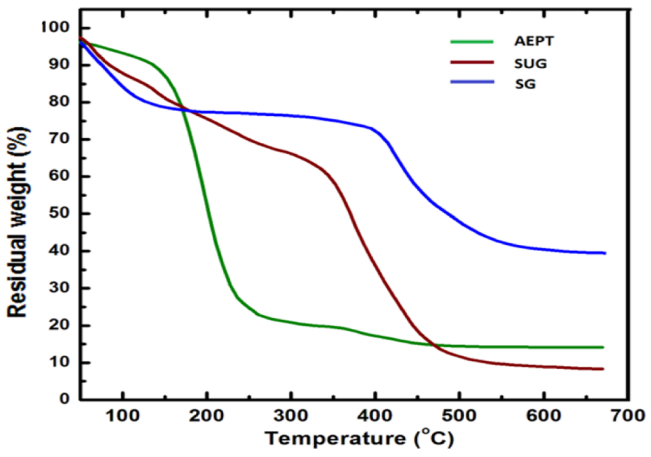

Figure 2. Thermogravimetric analysis of AEPT, SUG and SG analyzed from 37 to 680 °C at a ramp rate of 10 °C/min under nitrogen atmosphere. The results reported are based on the average of two different sets of experiments performed and scales from 50 to 680 °C.

SUG was observed to be thermally more stable compared to AEPT. The onset of degradation was noted around 360 °C. Interestingly, SG was found to be the most stable compared to AEPT and SUG. The higher percentage of degradation was observed in the beginning for AEPT, SUG and SG due to the loss of the adsorbed volatiles in every case. Apart from the degradation at lower temperatures, major weight loss was observed around 400 °C. Interestingly, both in the case of SG and SUG, the thermal stability was more compared to that of AEPT. This is due to (a) formation of thermally stable siloxane linkage, (b) improvement of barrier properties in heat transmission and insulation of the polymeric structure by the high aspect ratio filler material.[34] However, under similar experimental conditions, the thermal stability of the SG was superior compared to SUG. Macroscopically, the reason for differing thermal stability of polymer nanocomposite can be correlated to the concept of interparticle van der Waals interaction energy of the nanomaterials acting inside the polymeric phase. On the basis of the article by Israelachvili,[35] the van der Waals interaction energy (W) acting for two parallel plates separated by a distance D can be expressed as

$$W = -\frac{A}{12\pi D^2} \tag{5}$$

where A is the Hamaker constant, normally expressed as a product of $\pi^2 C\rho_1\rho_2$. Here, C is the coefficient of atom−atom pair potential and ρ_1 and ρ_2 are the number of atoms per unit volume. Thus, in the case of SG, the tethered polymeric chains are expected to increase the D value. As a result, the van der Waals interaction energy for the graphitic plates inside SG will be lower. This will lead to a better dispersed system. As a result, the graphitic surface will be more exposed to the polymeric system. When polymeric materials are subjected to high temperature, chain scission of the polymeric backbone occurs. As a result, free radicals are generated. However, in the presence of such exposed graphitic surfaces, the free radicals are scavenged in the medium. This causes better thermal stability of SG. Despite, the presence of graphitic platelets in the case of SUG, it has got a different thermal behavior compared to SG. This is attributed to the poor dispersion factor. Due to poor intercalation of the monomer chains inside the gallery spacing of pristine graphite, the van der Waals interaction energy value will be high enough to cause inter particle agglomeration. As a result, lesser number of graphitic structures will be exposed to the polymeric system. This justifies the increase in the thermal stability by 40 °C for SG compared to SUG. Because the estimation of grafting density was not possible by cleaving the polymer chains from the graphitic structure due to rapid formation of siloxane network, it was estimated from TGA by the procedure reported by Fang et al.[36] On the basis of the thermal analysis, a 32% grafting was achievable under the experimental conditions selected.

To further confirm the nature of dispersion, AFM was done in noncontact mode. Interestingly, the graphitic platelets were found to be well dispersed in the case of SG compared to SUG, as shown in Figure 3a,b. In line with the observation made in the AFM, the graphitic platelets for SUG appeared to be more agglomerated with less electron transparency when monitored using transmission electron microscopy (TEM). However, in the case of SG, the graphitic sheets appeared to be more electron transparent, thereby suggesting better dispersion and exfoliation of the graphitic platelets due to grafting of polymeric chains onto graphitic sheet as shown in Figure 3c,d.

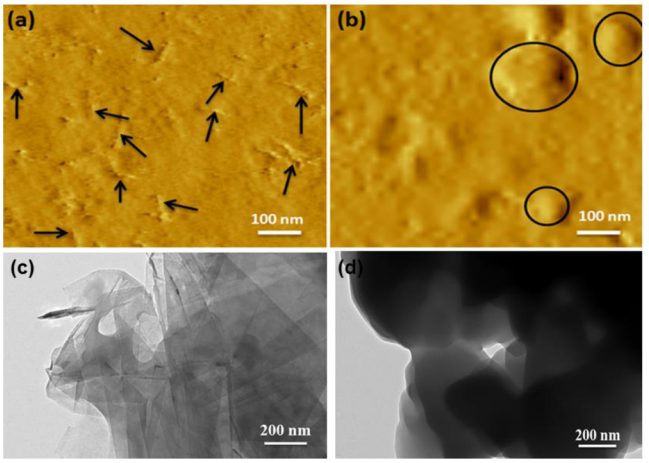

Figure 3. Noncontact mode AFM and HRTEM of (a) SG and (b) SUG surface.

To corroborate the results of AFM (about the dispersion of graphitic phase), current−voltage (I−V) characteristics for the neat polymers, SG and SUG were measured using a four probe technique at room temperature. In the range of experimental conditions selected, PAEPT was nonresponsive to the applied external DC voltage. It demonstrated an insulating character. However, a weak response for SUG and a strong electrical response for SG were noted, when a DC bias of up to 10 V was applied, as shown in Figure 4.

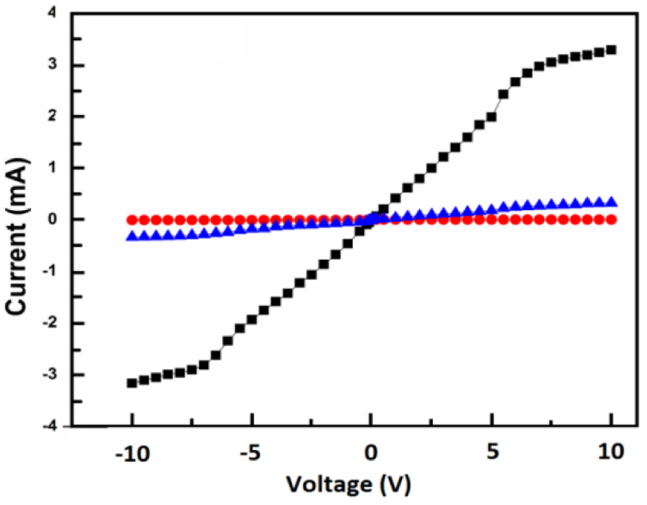

Figure 4. I−V characteristic curve of SG (black), SUG (blue) and PAEPT (red) observed in the range of −10 to +10 V using a four probe technique. Ten millimeter pellets for each sample were prepared using a pelletizer under a hydraulic press. The electrical response depicted here is based on average of data points obtained from two different sets of experiments.

In the window of study, SG exhibited an ohmic behavior. The conductivity for the SG was measured from the ohmic zone against a constant DC voltage of 5 V. This was found to be 2.41×10^{1} S/m. This value was substantially higher compared to the values obtained under similar loading of carbon nanofibers onto silicone polymer.[37] This is due to that fact that XG has a greater aspect ratio compared to carbon nanofibers. Thus, a lower fraction of filler loading is required while using graphitic plates as the nanophase for achieving

requisite percolation threshold value.[38] Despite the fact that that functionalization of graphitic system tends to open up the band gap of graphitic plates (insulating nature),[3] our composite showed a conducting nature. This is attributed to the selection of XG for the present system. The band gap of the XG and the pristine material was estimated using a scanning tunnelling spectroscopy technique by methods discussed elsewhere.[3] The degenerate π and π^* energy level (in the form of Dirac cones) at the Dirac point of graphene practically touch each other. As a result, we get zero band gap for expanded graphite.[3] However, any surface modification on graphitic materials tends to perturb the degeneracy present in the Dirac cones at the Dirac point.[3] As a result, the band gap of the functionalized material tends to open up due to covalent modification. The band gap of expanded graphite was almost zero and for XG, the band gap was obtained around 0.18 eV (semiconducting nature) as shown in the Supporting Information Figure S3. When monomer chains were tethered onto XG, the band gap of the XG does not change drastically. Further, the conductivity of polymer nanocomposites is largely guided by the dispersion and the nature of network formed by the nanophase inside the polymeric matrix.

In an attempt to understand the nature of dispersion of nanophase in the polymeric matrix, SEM analysis was done both on the surface as well as the fractured surface, as shown in Figure 5a–d. The dispersion of graphitic flakes was observed on

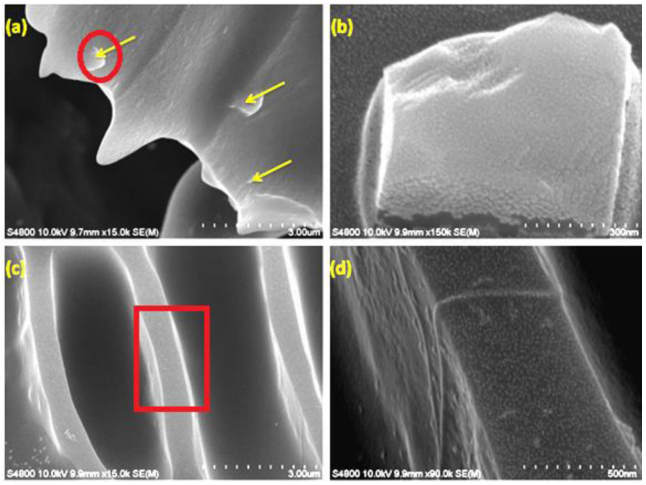

Figure 5. SEM images of SG at different magnification levels. (a) Surface of SG; yellow arrows indicates the graphitic particles on the surface of polymer at 15k magnification. (b) Morphology of graphitic plate on the surface of polymer matrix (particle encircled in red in panel a) at 150k magnification. (c) Fractured surface morphology of SG: the graphitic plates are perpendicular to the polymeric surface at regular interval recorded at 15k magnification. (d) Measurement of thickness of red boxed region (as shown in panel c) inside the polymeric matrix at 90k magnification.

the surface of the polymeric composite (Figure 5a,b). However, such a surface morphology was not sufficiently informative about the nature of the graphitic network formed inside the matrix. Thus, the surface of the polymeric composite was fractured in order to see the alignment of the graphitic plates (Figure 5c,d). On the basis of the reports present in the literature about the fractured surface of such polymer nanocomposites, the graphitic plates are observed to be aligned parallel to the surface of the polymer.[39] Similarly, in the present case, the graphitic plates were found to be parallel to the surface of the polymer, as shown in Figure 5c,d.

The observation made during fracture surface analysis of SG provides a hint for the formation of the hierarchical array of graphitic plates inside the polymeric matrix. The polymer wrapped graphitic plates were observed to have a thickness of around 500 nm. Such a hierarchical array results in formation of an electrically conducting network inside the polymeric matrix. As a result, SG showed ohmic response in the range of experimental conditions studied.

On the basis of such a structural observation, a hypothesis about the formation of hierarchical structure is shown in Scheme 2. The monomer chain initially got intercalated inside

Scheme 2. Proposed Scheme for Formation of Hierarchical Network of Functional Graphitic Plates Inside SG

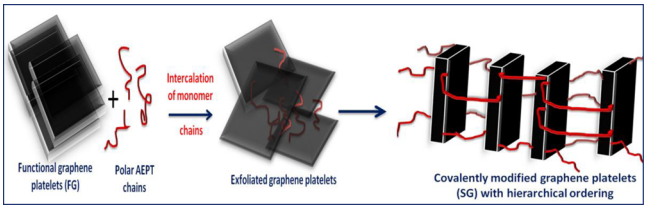

the graphitic basal plane and grafted onto the XG via amidation reaction (aided by DCC). These grafted AEPT units acted as a spacer, to effectively cause exfoliation of graphitic platelets in the case of SG. At a later stage, when the total system was exposed to moisture, these pendants polymerized and resulted in a matrix. However, for the unmodified carbon system, it was predicted that monomers will intercalate in between graphitic basal planes, but, reagglomeration of the graphitic structures will result due to the lack of any covalent bond between expanded graphite and monomer. This supports the observation made in AFM, wherein SG had a better dispersion compared to SUG.

To further investigate the essential differences present in the structure of PAEPT, SUG and SG, wide angle XRD was done, as shown in Figure 6. The XRD pattern of PAEPT constituted a broad halo at 2θ value of 20.1° This is due to presence of amorphous phase of the polymeric chains. The other notable peak was observed at 2θ value of 5°. This is due to room

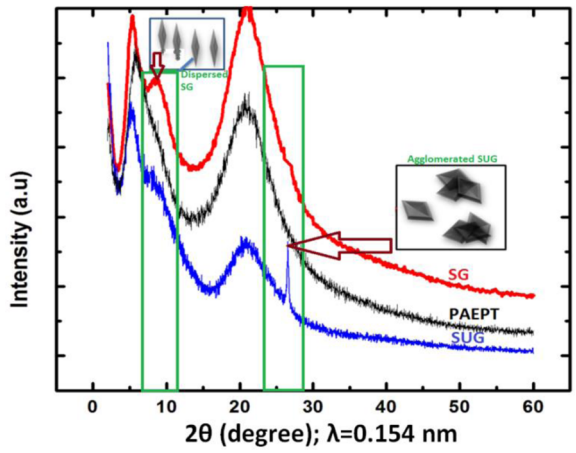

Figure 6. XRD pattern for PAEPT, SUG and SG using Cu Kα with λ = 0.154 nm.

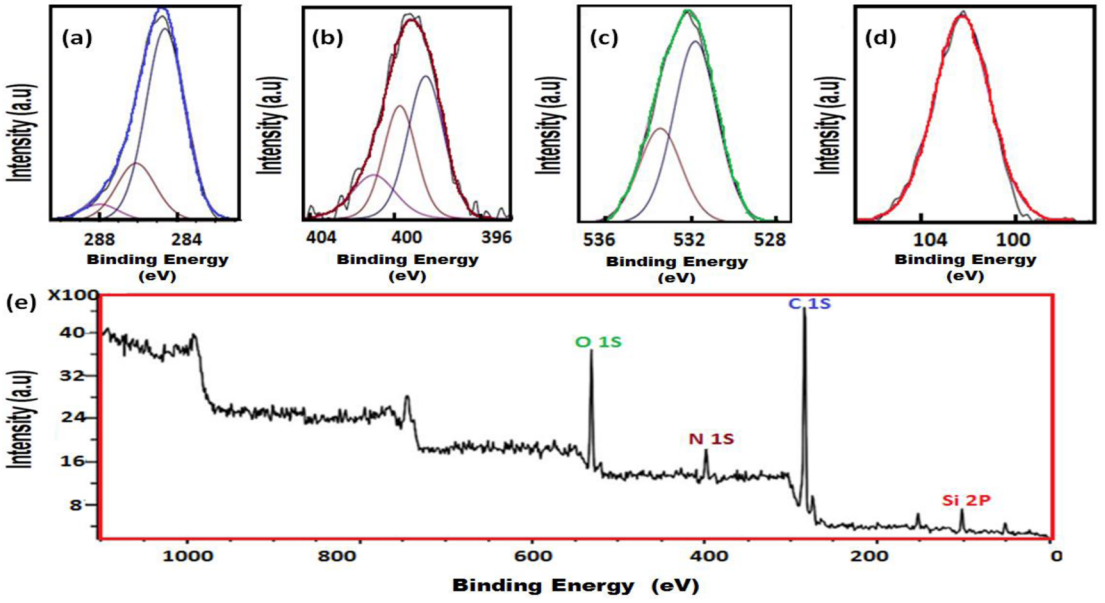

Figure 7. Deconvoluted high resolution XPS spectra of SG (a) C 1S; (b) N 1S; (c) O 1S; (d) Si 2p. (e) Typical survey scan of SG recorded using Mg Kα as the radiation source.

temperature crystallinity of the siloxane polymer. Similar diffraction patterns were observed for SUG and SG. However, for SUG, apart from the signature for the amorphous region, a sharp crystalline peak around 25° (graphitic 002 planes) was observed. This is due to the presence of unexfoliated graphitic particles. On the contrary, the scattering intensity at a 2θ value of 25° was absent for SG. However, a neck region was formed around the vicinity of a 2θ value of 8°. This authenticated about the exfoliation of graphitic layers. Hence, consistent with the the observation made by Potts et al.[40] about disappearance of crystalline peak of graphite due to exfoliation, SG had a better dispersion compared to SUG. Further, the tensile strength values obtained for SG and SUG were also in line with the results obtained in XRD. The tensile strength for SG was obtained as 120 kPa, whereas for SUG it was 30 kPa under similar loading. Similarly, the elongation at break was also increased to 40% for SG compared to 14% for SUG.

To corroborate the results obtained with a plausible reason for better dispersion and properties observed in the case of SG, an insight into the chemical changes taking place inside the matrix was desired. XPS was done to understand quantitatively the nature of bonds present inside the matrix as shown in Figure 7. A notable peak was observed at 284.6 eV, which corresponds to C 1s core electrons. The peaks at 286.1 and 288.0 eV correspond to C 1s carbon atoms attached to nitrogen and oxygen, respectively. The peaks at 521.82 and 533.43 eV are due to O 1s atoms attached to silicon and carbon atoms, respectively. The O/C ratio value for SG was obtained to be 21.71/76.31. Similarly, the peak observed at 102.3 eV infers the presence of silicon moiety in the grafted material. The Si/C ratio was found to be 1.24/76.31. The other notable peaks obtained were for nitrogen at 398.5 eV (nitrogen present in the chain of AEPT) and 399.7 eV (nitrogen in the amide bond grafted to graphitic plates) with an N/C ratio of 0.74/76.31. These results are consistent with our hypothesis of concurrent modification and formation of polymer matrix with its modifier AEPT.

On the basis of the report by Bhowmick and co-workers,[41] it has been proposed that the presence of nanomaterials inside an adhesive matrix increases the adhesive strength compared to the neat adhesive. Similar observations were reported by Coleman and co-workers,[42] where the incorporation of graphitic plates inside the adhesive matrix improved the adhesion property compared to the neat adhesive. In the present case, the adhesive property of SG was compared with that of SUG and PAEPT by using single lap shear measurements. Various materials were selected for checking the adhesion capability of the prepared sample. Glass−glass, and canvas−canvas samples were analyzed with PAEPT, SUG and SG. Cohesive failure in the case of the glass surface was observed (below a force value of 7.2 N). However, a different trend was observed for canvas cloth. The lap shear strength for PAEPT and SUG samples was 1086 and 1121 N/m^2, respectively, whereas the same for SG increased to 1250 N/m^2, as shown in Figure 8.

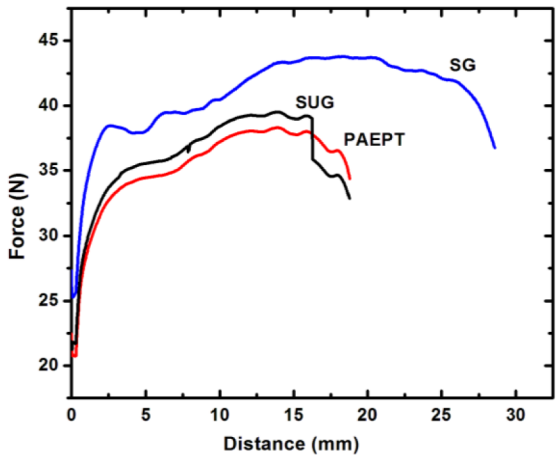

Figure 8. Force vs distance plot for canvas−canvas sample treated with PAEPT (red), SUG (black) and SG (blue) done in single lap shear mode. The samples were kept under adhesion conditions for 10 h using a load of 2 kg. A 50 N load cell was used for this test with a speed of 25 mm/min.

The cohesive failure for glass samples is attributed to the fact that silane based polymer has a strong affinity toward the surface of glass. As a result, under the selected experimental conditions, there was a cohesive failure. In the case of canvas, however, SG exhibited superior properties compared to PAEPT. To find out the governing factor for such an effect, the water contact angle was measured, as shown in Figure 9.

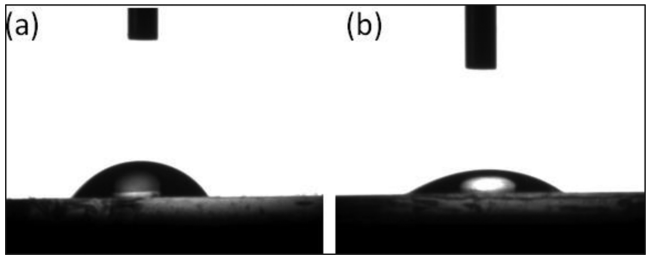

Figure 9. Water contact angle measurement done using pendant drop method on (a) PAEPT and (b) SG.

The water contact angle measurements value for PAEPT was in the vicinity of 47°, whereas for SG, it dropped down to 39°. The decrease in the water contact angle for SG is ascribed to the presence of amide bond. On the basis of the water contact angle value, SG will have a better surface wettability compared to PAEPT. As a result, the adhesion force acting on the surface of substrate will be higher when SG is used over PAEPT. Further, the roughness of the adhesive surface also plays a critical role in determining the strength of adhesion. In the present case, the surface of SG is expected to be coarser (R_a = 136 ± 1 nm; calculated using ImageJ software, Version 1.48, NIH, USA) compared to PAEPT. As a result, it is expected to act as a better adhesive. Further, incorporation of graphitic particles increases the bond breaking resistance at the adhesion points. As a result, the value of bond strength increases for SG compared to PAEPT.

CONCLUDING REMARKS

We have demonstrated that successful grafting of [3-(2-aminoethylamino)propyl]trimethoxysilane onto functionalized graphitic plates (with a low band gap) was achieved using the "grafting to" methodology. The adopted route for functionalization resulted in the formation of a well dispersed nanophase inside the polymeric matrix. As a result, a better electrical response was observed for the grafted composite over the physical mixture. The functionalized material needed no external curing agent. Further the conducting composite so generated acted as an instant adhesive. The adhesion property of the composite was found to be better compared to that of the neat adhesive. The adhesive and conducting nature of the present polymer nanocomposite makes it a promising candidate for electrically conducting adhesives. Further, it can be envisioned that, utilizing this strategy, a graphitic platelets based conducting adhesive can be developed for interconnecting subcells of tandem solar cells.

ASSOCIATED CONTENT

Supporting Information

Mechanism of Scheme 1, selective area FTIR spectra, Raman spectra and STS plot of d[ln I/d[ln V] versus voltage for pristine expanded graphite and XG. This material is available free of charge via the Internet at http://pubs.acs.org.

AUTHOR INFORMATION

Corresponding Authors

*A. K. Bhowmick. E-mail: anilkb@rtc.iitkgp.ernet.in.
*R. Krishnamoorti. E-mail: ramanan@uh.edu.

Author Contributions

T.M., A.K.B. and R.K. designed the experiments. T.M. performed the experiments and analyzed the data. T.M., A.K.B. and R.K. contributed to the understanding of the results and the writing of the paper.

Notes

The authors declare no competing financial interest.

ACKNOWLEDGMENTS

The authors acknowledge Indo-US Science and Technology Forum (IUSSTF) for their support. Mondal et al. acknowledges the help of Dr. Biswarup Satpati, Surface Physics Devision, Saha Institute of Nuclear Physics, Kolkata, India for TEM experiments. R.K. acknowledges the partial support of the Gulf of Mexico Research Initiative (Consortium for Ocean Leadership Grant SA 12-05/GoMRI-002).

REFERENCES

(1) Geim, A. K.; Novoselov, K. S. Rise of Graphene. *Nat. Mater.* **2007**, *6*, 183−191.
(2) Schweirz, F. Graphene Transistors. *Nat. Nanotechnol.* **2010**, *5*, 487−496.
(3) Mondal, T.; Bhowmick, A. K.; Krishnamoorti, R. Stress Generation and Tailoring of Electronic Properties of Expanded Graphite by Click Chemistry. *ACS Appl. Mater. Interfaces* **2014**, *6*, 7244−7253.
(4) Liu, J.; Xue, Y.; Dai, L. Sulfated Graphene Oxide as a Hole-Extraction Layer in High-Performance Polymer Solar Cells. *J. Phys. Chem. Lett.* **2012**, *3*, 1928−1933.
(5) Beckert, F.; Rostas, A. M.; Thomann, R.; Weber, S.; Schleicher, E.; Friedrich, C.; Mulhaupt, R. Self-Initiated Free Radical Grafting of Styrene Homo- and Copolymers onto Functionalized Graphene. *Macromolecules* **2013**, *46*, 5488−5496.
(6) Qi, X.-Y.; Yan, D.; Jian, Z.; Cao, Y.-K.; Yu, Z.-Z.; Yavari, F.; Koratkar, N. Enhanced Electrical Conductivity in Polystyrene Nanocomposites at Ultra-Low Graphene Content. *ACS Appl. Mater. Interfaces* **2011**, *3*, 3130−3133.
(7) Cheng, S.; Chen, X.; Hsuan, Y. G.; Li, C. Y. Reduced Graphene Oxide-Induced Crystallization in Solution and Nanocomposites. *Macromolecules* **2012**, *45*, 993−1000.
(8) Mondal, T.; Bhowmick, A. K.; Krishnamoorti, R. Chlorophenyl Pendant Decorated Graphene Sheet as a Potential Antimicrobial Agent: Synthesis and Characterization. *J. Mater. Chem.* **2012**, *22*, 22481−22487.
(9) Pernites, R.; Vergara, A.; Yago, A.; Cui, K.; Advincula, R. C. Facile Approach to Graphene Oxide and Poly(*N*-vinylcarbazole) Electro-Patterned Films. *Chem. Commun.* **2011**, *47*, 9810−9812.
(10) Kim, H.; Abdala, A. A.; Macosko, C. W. Graphene/Polymer Nanocomposites. *Macromolecules* **2010**, *43*, 6515−6530.
(11) Castelain, M.; Martinez, G.; Marco, C.; Ellis, G.; Salavagione, H. J. Effect of Click-Chemistry Approaches for Graphene Modification on the Electrical, Thermal, and Mechanical Properties of Polyethylene/Graphene Nanocomposites. *Macromolecules* **2013**, *46*, 8980−8987.
(12) Tang, Z.; Kang, H.; Shen, Z.; Guo, B.; Zhang, L.; Jia, D. Grafting of Polyester onto Graphene for Electrically and Thermally Conductive Composites. *Macromolecules* **2012**, *45*, 3444−3451.
(13) Zheng, H.; Gao, C.; Wang, Y.; Watts, P. C. P.; Kong, H.; Liu, X.; Yan, D. In Situ Polymerization Approach to Multiwalled Carbon Nanotubes-Reinforced Nylon 1010 Composites: Mechanical Properties and Crystallization Behavior. *Polymer* **2006**, *47*, 113−122.
(14) Das, S.; Wajid, A. S.; Shelburne, J. L.; Lia, Y.-C.; Green, M. J. Localized In situ Polymerization on Graphene Surfaces for Stabilized

Graphene Dispersions. *ACS Appl. Mater. Interfaces* **2011**, *3*, 1844−1851.
(15) Dreyer, D. R.; Park, S.; Bielawski, C. W.; Ruoff, R. S. The Chemistry of Graphene Oxide. *Chem. Soc. Rev.* **2010**, *39*, 228−240.
(16) *Polymer Nanocomposites: Synthesis, Characterization and Modeling*; Krishnamoorti, R.; Vaia, R. A., Eds.; ACS Symposium Series; American Chemical Society: Washington, DC, 2002, 804.
(17) Yim, M. J.; Li, Y.; Moon, K.-S.; Paik, K. W.; Wong, C. P. Review of Recent Advances in Electrically ConductiveAdhesive Materials and Technologies in Electronic Packaging. *J. Adhes. Sci. Technol.* **2008**, *22*, 1593−1630.
(18) Leong, C.-K.; Chung, D. D. L. Electrically Conductive Acrylic Pressure-Sensitive Adhesives Containing Carbon Black. *J. Electron. Mater.* **2004**, *33*, 203−206.
(19) Gojny, F. H.; Wichmann, M. H. G.; Fiedler, B.; Kinloch, I. A.; Schulte, K. Evaluation and Identification of Electrical and Thermal Conduction Mechanisms in Carbon Nanotube/Epoxy Composites. *Polymer* **2006**, *47*, 2036−2045.
(20) Pu, N.-W.; Peng, Y.-Y.; Wang, P.-C.; Chen, C.-Y.; Shi, J.-N.; Liu, Y.-M.; Ger, M.-D.; Chang, C.-L. Application of Nitrogen-Doped Graphene Nanosheets in Electrically Conductive Adhesives. *Carbon* **2014**, *67*, 449−456.
(21) Yu, A.; Ramesh, P.; Itkis, M. E.; Bekyarova, E.; Haddon, R. C. Graphite Nanoplatelet−Epoxy Composite Thermal Interface Materials. *J. Phys. Chem. C* **2007**, *111*, 7565−7569.
(22) Raza, M. A.; Westwood, A. K.; Brown, A. P.; Stirling, C. Texture, Transport and Mechanical Properties of Graphite Nanoplatelet/Silicone Composites Produced by Three Roll Mill. *Compos. Sci. Technol.* **2012**, *72*, 467−475.
(23) Tung, V. C.; Kim, J.; Cote, L. J.; Huang, J. Sticky Interconnect for Solution-Processed Tandem Solar Cells. *J. Am. Chem. Soc.* **2011**, *133*, 9262−9265.
(24) Choi, J.-Y.; Kim, S. W.; Cho, K. Y. Improved Thermal Conductivity of Graphene Encapsulated Poly(methyl methacrylate) Nanocomposite Adhesives with Low Loading Amount of Graphene. *Compos. Sci. Technol.* **2014**, *94*, 147−154.
(25) Sydlik, S. A.; Lee, J.-H.; Walish, J. J.; Thomas, E. L.; Swager, T. M. Epoxy Functionalized Multi-Walled Carbon Nanotubes for Improved Adhesives. *Carbon* **2013**, *59*, 109−120.
(26) Zhu, J.; Kim, J.; Peng, H.; Margrave, J. L.; Khabashesku, V. N.; Barrera, E. V. Improving the Dispersion and Integration of Single-Walled Carbon Nanotubes in Epoxy Composites through Functionalization. *Nano Lett.* **2003**, *3*, 1107−1113.
(27) Bissett, M. A.; Tsuji, M.; Ago, H. Mechanical Strain of Chemically Functionalized Chemical Vapor Deposition Grown Graphene. *J. Phys. Chem. C* **2013**, *117*, 3152−3159.
(28) Mondal, T.; Bhowmick, A. K.; Krishnamoorti, R. Synthesis and Characterization of Bi-Functionalized Graphene and Expanded Graphite Using n-Butyl Lithium and Their Use for Efficient Water Soluble Dye Adsorption. *J. Mater. Chem. A* **2013**, *1*, 8144−8153.
(29) Fotea, C.; D'Silva, C. The Use of Silane Reagents as Primers to Enhance the Adhesion of Chromium Tanned Heavy-Duty Leather (Salz Leather). *Int. J. Adhes. Adhes.* **2004**, *24*, 1.
(30) Vanlandingham, M. R.; Edulijee, R. F.; Gillespie, J. W., Jr. Moisture Diffusion in Epoxy Systems. *J. Appl. Polym. Sci.* **1999**, *71*, 787−798.
(31) Mackay, M. E.; Tuteja, A.; Dluxbury, P. M.; Hanker, C. J.; Horn, B. V.; Guan, Z.; Chen, G.; Krishnan, R. S. General Strategies for Nanoparticle Dispersion. *Science* **2011**, *311*, 1740−1743.
(32) Hooper, J. B.; Schweizer, K. S. Theory of Phase Separation in Polymer Nanocomposite. *Macromolecules* **2006**, *39*, 5133−5142.
(33) Fowkes, F. M.; Tischler, D. O.; Wolfe, J. A.; Lannigan, L. A.; John, C. M. A.; Halliwell, M. J. Acid Base Complexes of Polymers. *J. Polym. Sci., Part A: Polym. Chem.* **1984**, *22*, 547−566.
(34) Roy, N.; Bhowmick, A. K. Tailor-Made Fibrous Nanohydroxyapatite/Polydimethylsiloxane Composites: Excavating the Role of Nanofiller Aspect Ratio, Amorphicity, and Noncovalent Surface Interaction. *J. Phys. Chem. C* **2012**, *116*, 8763−8772.
(35) Israelachvili, J. N. *Intermolecular and Surface Forces*, 3rd ed; Academic Press: San Diego, CA, 2011.
(36) Fang, M.; Wang, K.; Lu, H.; Yang, Y.; Nutt, S. Covalent Polymer Functionalization of Graphene Nanosheets and Mechanical Properties of Composites. *J. Mater. Chem.* **2009**, *19*, 7098−7105.
(37) Roy, N.; Bhowmick, A. K. In situ Preparation, Morphology and Electrical Properties of Carbon Nanofiber/Poly-dimethylsiloxane Nanocomposites. *J. Mater. Sci.* **2012**, *47*, 272−281.
(38) He, L.; Tjong, S. C. Low Percolation Threshold of Graphene/Polymer Composites prepared by Solvothermal Reduction of Graphene Oxide in the Polymer Solution. *Nano. Res. Lett.* **2013**, *8*, 132−139.
(39) Sakurai, S. I.; Okoshi, K.; Kumaki, J.; Yahsima, E. Two-Dimensional Hierarchical Self-Assembly of One-Handed Helical Polymers on Graphite. *Angew. Chem., Int. Ed.* **2006**, *45*, 1245−1248.
(40) Potts, J. R.; Murali, S.; Zhu, Y.; Zhao, X.; Ruoff, R. S. Microwave-Exfoliated Graphite Oxide/Polycarbonate Composites. *Macromolecules* **2011**, *44*, 6488−6495.
(41) Basak, G. C.; Kumar, K. D.; Bandyopadhyay, A.; Bhowmick, A. K. Elegant Way of Strengthening Polymer−Polymer Interface Using Nanoclay. *ACS Appl. Mater. Interfaces* **2010**, *2*, 2933−2943.
(42) Khan, U.; May, P.; Porwal, H.; Nawaz, K.; Coleman, J. N. Improved Adhesive Strength and Toughness of Polyvinyl Acetate Glue on Addition of Small Quantities of Graphene. *ACS Appl. Mater. Interfaces* **2013**, *5*, 1423−1428.